06 Oct 1971

Turbulence Measurements with the Split-Film Anemometer Probe

B. W. Spencer

B. G. Jones

TURBULENCE MEASUREMENTS WITH THE SPLIT-FILM ANEMOMETER PROBE

Bruce W. Spencer* and Barclay G. Jones

Nuclear Engineering Program
University of Illinois at Urbana-Champaign
Urbana, Illinois 61801

ABSTRACT

The newly developed split-film anemometer probe, manufactured by Thermo-Systems, Inc. of St. Paul, Minnesota, has been applied to the measurement of two-dimensional turbulence characteristics, including turbulent shear stress, in mixing layer and boundary layer shear flows. Probes of both 6-mil and 2-mil diameters were used which had the same physical dimensions as ordinary hot-film anemometer probes. The film on this sensor is split into two 170° elements resulting in two independent sensors. This enables the probe to detect vertical as well as axial components of the instantaneous velocity vector. It therefore serves the same purpose as an x-probe, but because of its very small size it has significant advantages in regions of very high shear, particularly in the region close to the wall in the boundary layer. The response equations used to evaluate flow characteristics from the anemometer signals are presented. Operating features such as frequency response, aximuthal yaw sensitivity, signal-to-noise, and stability are discussed and comparisons are made with those of an x-probe. Measurements in turbulent air flow using a hot-wire, x-probe, and split-film probe are presented and the performance of the latter is discussed. The results show that the split-film probe is a promising device for measuring two-dimensional turbulence information, particularly when high transverse spatial resolution is required. However, until improvements can be made, adequate frequency response should be verified by the experimenter for each flow regime of anticipated use.

INTRODUCTION

The split-film anemometer sensor, recently developed by Thermo-Systems Inc. (TSI) for their total vector anemometer system,[1] has been applied to two-dimensional velocity measurements in turbulent shear flow. This unique sensor has the same physical characteristics as ordinary 6-mil and 2-mil sensors presently used for hot-film probes; however, the sensitive film has been split longitudinally into two separate sensor elements (Fig. 1) providing the ability

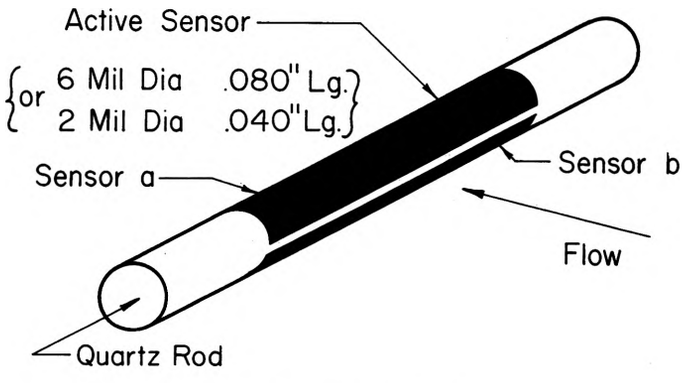

Figure 1 - Schematic of Split-Film Anemometer Sensor

to monitor the transverse as well as axial components of the local velocity vector. Consequently, for the measurements described in this investigation, the probe has the same utility as an x-configuration probe. Its important advantage is its much smaller physical size in the direction of the mean shear, being simply the 6-mil or 2-mil diameter of the sensor itself. This minimizes spatial averaging in regions of severe velocity gradient, and allows two-dimensional turbulence quantities, including shear stress, to be measured much closer to a surface than is possible with an x-probe. The split-film probe is therefore particularly attractive for boundary layer studies. As is characteristic of hot-film sensors, the probe is rugged and utilizes straightforward response equations. On the other hand, initial purchase and repair of a damaged sensor are more costly than for a conventional x-probe using wire or film sensors.

THEORY OF OPERATION

The theory of operation for two-dimensional velocity sensing is based on the non-uniform heat transfer distribution around a heated cylinder in cross flow. The distribution of the local heat transfer coefficient is shown schematically in Fig. 2. It can be seen that maximum heat transfer occurs in

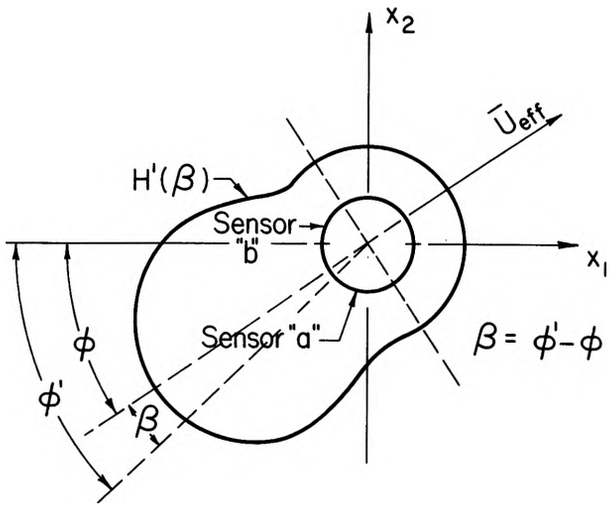

Figure 2 - Schematic of Local Heat Transfer Coefficient Distribution Around a Circular Cylinder

the region of upstream stagnation. It is tacitly assumed that this distribution follows rapidly the fast changes in the velocity azimuthal direction, ϕ. Sensors a and b in Fig. 2 respond independently to the heat flux averaged azimuthally over their respective surfaces. The sensors are held at constant and nominally identical temperatures using two channels of standard constant-temperature anemometry. Proper combination of the output voltages of these two networks will provide signals yielding both the axial and transverse components of the velocity vector. The experimenter has wide latitude in selecting accuracy versus simplicity using this probe, depending upon the form of the response equations selected and the types of analog and/or digital instrumentation available for data processing. In general, assuming adequate frequency response, accuracy is equivalent to that of the standard x-probe, and may even be substantially improved using certain techniques to be described. The remainder of this section and the following section describe how the response equations are obtained analytically.

*Present address: Argonne National Laboratory, Argonne, Illinois

Consider a split-film sensor oriented in a flow field as illustrated in Fig. 3. We will use a standard right-hand orthogonal coordinate system with

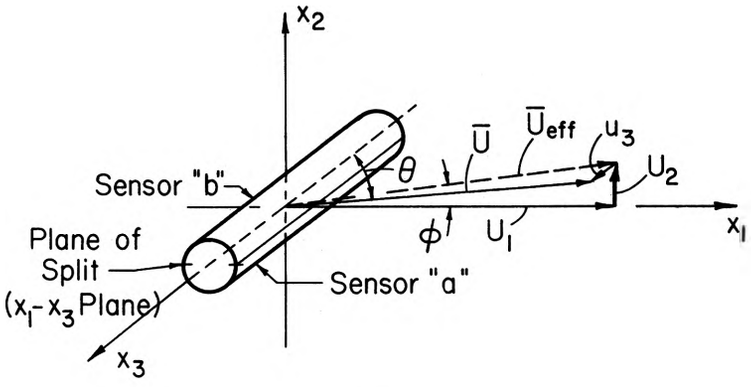

Figure 3 - Orientation of Split-Film Sensor in Flow Field

directions x_i, i = 1, 2, 3, associated with velocity components U_i. The direction x_1 is the axial or main flow direction, x_2 is the transverse direction (the mean shear direction), and x_3 is a direction of symmetry coinciding with the sensor axis. We use the convention that upper case symbols represent instantaneous total values, lower case symbols denote instantaneous fluctuations whose time averages are zero, and overscored symbols represent time averaged quantities. The sensor split is assumed to be ideally aligned with the x_1-x_3 plane; the flow is assumed to be isothermal and incompressible. The local velocity vector is represented by:

$$\vec{U} = (\bar{U}_1 + u_1)\hat{x}_1 + (\bar{U}_2 + u_2)\hat{x}_2 + u_3\hat{x}_3 \tag{1}$$

and

$$U = |\vec{U}| = \bar{U}_1\left[(1 + \frac{u_1}{\bar{U}_1})^2 + (\frac{\bar{U}_2 + u_2}{\bar{U}_1})^2 + (\frac{u_3}{\bar{U}_1})^2\right]^{\frac{1}{2}} \tag{2}$$

The effective cooling velocity, defined as that component of the vector $\vec{U}$ influencing the sensor heat transfer and thereby contributing to the measured anemometer signals, is given by:

$$\vec{U}_{eff} = (\bar{U}_1 + u_1)\hat{x}_1 + (\bar{U}_2 + u_2)\hat{x}_2 \tag{3}$$

and

$$U_{eff} = |\vec{U}_{eff}| = \bar{U}_1\left[(1 + \frac{u_1}{\bar{U}_1})^2 + (\frac{\bar{U}_2 + u_2}{\bar{U}_1})^2\right]^{\frac{1}{2}} \tag{4}$$

The assumption made here is that the velocity component parallel to the sensor axis has negligible cooling effect. This is valid for film sensors of even small length-to-diameter ratios when they are oriented normal to the flow direction as is the case for the split-film sensor. (Note, however, that this simplification could not be made in analyzing an x-configuration film probe where deviations from sine law cooling are significant due to the inclined orientation of the sensor. This is an additional advantage of the split-film sensor for high intensity applications.)

The power dissipated in sensor i is given by:

$$Q_i = I_i^2 R_i = h_i(U_{eff}, \phi)\, A_i(T_{S_i} - T_a) \tag{5}$$

in which the end conduction losses have been neglected and where, for sensor i, I_i is the sensor current, R_i is the sensor resistance at temperature T_{S_i}, h_i is the convective heat transfer coefficient averaged over the surface of the sensor, A_i is its surface area, and T_a is the ambient fluid temperature. For a constant temperature anemometer network, the quantity $A_i(T_{S_i} - T_a)$ is constant, and its value is not important for present considerations.

The convective heat transfer coefficient h_i may be expressed in the following form:

$$h_i(U_{eff}, \phi) = (A + B\, U_{eff}^n) f(\phi) \tag{6}$$

The first factor on the right-hand-side shows the dependency on velocity magnitude (from the familiar King's law), and $f(\phi)$ is an additional factor representing the azimuthal cooling variation. This can be evaluated from knowledge of the azimuthal distribution of h_i shown in Fig. 2. Unfortunately, to the knowledge of the authors, there is no data for $h(\phi)$ in the Reynolds number range of interest ($10^{-2} < Re < 10^3$), although this is presently being studied.[2] Kreith[3] gives data at $Re > 10^4$ which, in the absence of more appropriate data, will be used here. The empirical representation is (see Fig. 2):

$$h'(\beta) \propto 1 - (|\beta|/90)^3;\ 0 \le |\beta| \le 80^\circ \tag{7a}$$

and

$$h'(\beta) = \text{constant};\ 80 < |\beta| \le 180^\circ \tag{7b}$$

where $\beta = \phi' - \phi$. The instantaneous surface averaged coefficients for sensors a and b are given by:

$$h_a(\phi) = \int_0^{180} h'(\phi' - \phi)\, d\phi' \tag{8a}$$

and

$$h_b(\phi) = \int_{180}^{360} h'(\phi' - \phi)\, d\phi' \tag{8b}$$

In actuality, allowance should be made for the split width of approximately 1/2 mil when taking the limits for these integrals. *Figure 4 shows* the results

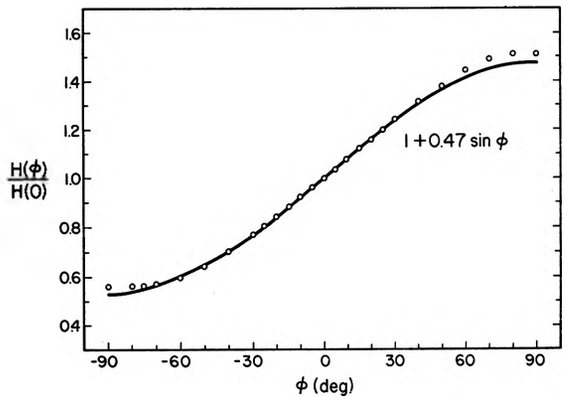

Figure 4 - Azimuthal Variation of Surface Averaged Heat Transfer Coefficient

of these integrations using Eqs. (7a) and (7b). The azimuthal cooling factor $f_i(\phi) = h_i(\phi)/h_i(o)$ is seen to be approximated well in the range $|\phi| \le 50^\circ$ by the simple expression:

$$f_i(\phi) = 1 + \alpha_i \sin\phi \tag{9}$$

where $|\phi_i| = 0.47$. The basic validity of this relation was demonstrated by azimuthal yaw calibration as will be shown in the following section. From the geometry of the vector field, it is evident that:

$$\sin\phi = U_2/U_{eff} \tag{10}$$

and, therefore, using Eqs. (5) and (6):

$$Q_i = \text{constant} \times (A + B\, U_{eff}^n)(1 + \alpha_i \frac{U_2}{U_{eff}}) \tag{11}$$

This equation relates the power dissipated in sensor i to the two-dimensional flow field characteristics. To evaluate the flow field components we must

relate the sensor heat transfer given by Eq. 11 to the measurable anemometer voltages in a convenient form.

Response Equations

Several approaches can be taken in deriving response equations depending on the accuracy desired. We will start with the most exact form (and most difficult to implement) and make simplifications leading to a form analogous to the familiar x-array equations applicable for low intensity turbulence. Certain assumptions are made throughout, notably that the temperatures of sensors a and b are matched (to avoid net heat exchange between sensors), that the power circuit calibrations are matched via appropriate electronics, and that angular sensitivities are matched ($\alpha_a = -\alpha_b \equiv \alpha$) via proper sensor orientation.

The power dissipated by sensor i is given by Eq. 11. A voltage proportional to this power is obtainable by squaring the anemometer bridge voltage (through the first squaring circuit of commercially available linearizers for example.). Subtracting electronically the zero flow voltage, we have for the i^{th} channel:

$$E_{p_i} = K_{p_i} (Q - Q_o)_i = K_{p_i} U_{eff}^n \left(1 + \alpha_i \frac{U_2}{U_{eff}}\right) \tag{12}$$

where K_{p_i} is a calibration constant for the i^{th} sensor. This is the basic power circuit equation for the split-film sensor.

Case 1.- The power circuit signals, Eq. 12, may be summed and differenced directly to yield, respectively, noting that $K_{p_i} = K_p$ and $\alpha_i = \alpha$ for matched conditions,

$$E_s = G_s(E_{p_a} + E_{p_b}) = 2 G_s K_p U_{eff}^n \tag{13}$$

and

$$E_d = G_d(E_{p_a} - E_{p_b}) = 2 G_d K_p \alpha U_{eff}^{n-1} U_2 \tag{14}$$

For cylinders oriented normally to the flow, the exponent n is found, to a first approximation, to be 0.5 for $Re \geq 45$, and the product $E_p = G_p E_s E_d$ is a linear function of the transverse velocity component U_2 alone; ie,

$$E_p = G_p E_s E_d = 4 K_p^2 G_s G_d G_p \alpha U_2 = S_2 U_2$$

When n is not 0.5 the sensitivity is not constant but is a function of U_{eff}. This may be avoided by treating the sum and difference signals by suitable conditioning to have n = 0.5. Thus:

$$\overline{U}_2 = (1/S_2)\, \overline{E}_p \text{ and } u_2 = (1/S_2)\, e_p \tag{15}$$

The sensitivity S_2 is determined readily from direct azimuthal yaw calibration. For convenience, the summed circuit may be linearized yielding:

$$E_\ell = G_\ell E_s^{1/n} = G_\ell (2 G_s K_p)^{1/n} U_{eff} = S_1 U_{eff} \tag{16}$$

The sensitivity S_1 may also be determined from calibration. Since $U_{eff}^2 = U_1^2 + U_2^2$, and since U_2 is known exactly from Eq. 15, the instantaneous two-dimensional flow field can be evaluated. This would most readily be accomplished using digital data analysis techniques since the analog equipment required would be cumbersome. However, it is apparent that high accuracy two-dimensional measurements are possible using this approach even in high intensity turbulence. Accuracy would be dependent only on the basic assumptions of rapid azimuthal cooling variation, sine-law azimuthal cooling (Eq. 9), matched circuits, and n = 0.5.

Case 2.- For laboratory measurements it is desirable to monitor the flow field characteristics using available analog instrumentation and familiar anemometry techniques. We will assume that the local turbulence intensity is sufficiently small to neglect velocity fluctuations of 2nd and higher orders. (This is essentially the familiar "low intensity" assumption for x-probe anemometry.) Expanding U_{eff} in Eq. 14, and assuming additionally that n = 0.5 and $\overline{U}_2/\overline{U}_1 \ll 1$:

$$E_d = 2 G_d K_p \alpha U_2 \overline{U}_1^{-\frac{1}{2}}$$

Therefore,

$$\overline{U}_2 = (S_2 \overline{U}_1^{-\frac{1}{2}})^{-1} \overline{E}_d \text{ and } u_2 = (S_2 \overline{U}_1^{-\frac{1}{2}})^{-1} e_d \tag{17}$$

The method of calibration is suggested by the basic difference equation, Eq. 14, rewritten here in the form:

$$\frac{\overline{U}_2}{\overline{U}_{eff}} = \sin\phi = \frac{1}{S} \frac{\overline{E}_d}{\overline{U}_{eff}^n} \tag{18}$$

for time-averaged values. Azimuthal yaw calibration data are shown in Fig. 5

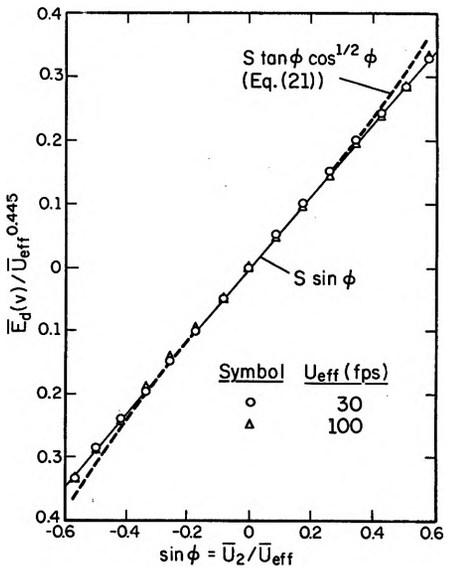

Figure 5 - Azimuthal Yaw Calibration for SF-6 in Air Flow at 30 and 100 fps with O.H.R. = 1.5

supporting this result. These data were obtained using a 6-mil split-film sensor (SF-6) at an overheat ratio of 1.5 in smooth wind tunnel flow (background turbulence intensity was nominally 0.1%). The purpose of the yaw calibration is threefold: 1) to establish the limits of validity of Eq. 14; 2) to determine the best exponent n for data reduction; and 3) to determine the sensitivity S for a given experimental setup. Data reduction showed the best agreement with an exponent of n = 0.445. Agreement of the yaw data with its analytical representation, sin ϕ, is seen to be excellent over the range of angles $\phi = \pm 35^\circ$. Larger angles were not possible using the apparatus available, although as shown above, it is anticipated that agreement would be good to $\phi = \pm 50^\circ$.

For the low intensity approximation, Eq. 17 is rewritten:

$$\frac{\overline{U}_2}{\overline{U}_1} = \tan\phi = \frac{1}{S} \frac{\overline{E}_d}{\overline{U}_1^{\frac{1}{2}}} \tag{19}$$

Since U_{eff}, rather than U_1, is set during a yaw calibration, the analytical representation corresponding to the low intensity approximation is given by:

$$\frac{\overline{U}_2}{\overline{U}_1} = \frac{1}{S} \frac{\overline{E}_d}{\overline{U}_{eff}^{\frac{1}{2}} \cos^{\frac{1}{2}}\phi} \tag{20}$$

so that

$$\frac{\overline{E}_d}{\overline{U}_{eff}^{1/2}} = S \tan\phi \cos^{1/2}\phi \qquad (21)$$

The right-hand side of Eq. 21 is also plotted on Fig. 5 and shows excellent agreement with data in the range $|\phi| \lesssim 25^o$. The instantaneous angle $\phi = 25^o$ would be seen by the sensor less than 5% of the time (assuming Gaussian statistics and $\pm$ two standard deviations) for transverse intensities $u_2'/\overline{U}_1 \approx 0.25$ (prime denotes rms). This may be considered to define the limit of applicability of the methods of Case II.

To obtain U_1 it is again convenient to linearize the "summed" power circuit. Using a first order expansion for U_{eff} in Eq. 16 and assuming n = 0.5, we obtain:

$$E_\ell = S_1\overline{U}_1\left[1 + \frac{u_1}{\overline{U}_1}\right] \qquad (22)$$

and from this we find:

$$\overline{U}_1 = (1/S_1)\overline{E}_\ell \text{ and } u_1 = (1/S_1)e_\ell \qquad (23)$$

The sensitivity, S_1, is obtained from calibration in the velocity interval of interest. The voltage, E_ℓ, was found to be insensitive to azimuthal yaw as anticipated. The maximum deviation from $E_\ell(\phi = 0)$ in the range $\phi = \pm 35^o$ was less than 4%. A simple circuit diagram for these measurements is shown in Fig. 6. This network, and the response Equations 17 and 23, were used for the boundary layer turbulence measurements described later.

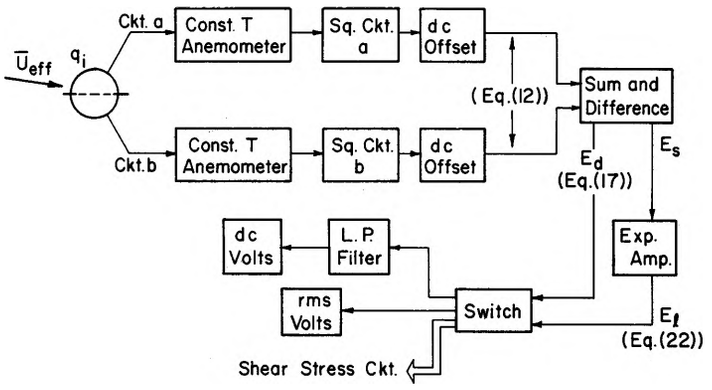

Figure 6 - Component Block Diagram for Case II

An error analysis for the techniques described in Case 2 can be made by including 2nd order terms in the series expansions for the response equations. The results, when compared with a similar analysis for an x-array, show $u_1/\overline{U}_1$ to be measured somewhat more accurately with the split-film probe (errors of order 1/2 $u_2^2/\overline{U}_1^2$ vs. $u_3^2/\overline{U}_1^2$ for the split-film and x-array, respectively) while $u_2/\overline{U}_1$, on the other hand, is measured more accurately with the x-array (error of order 1/2 $u_1^2/\overline{U}_1^2$ vs. $u_1^3/\overline{U}_1^3$ for the split-film and x-array, respectively). This shows that one sacrifices little in accuracy using the split-film probe and the "low-intensity" response equations compared with the available accuracy for the x-probe.

Case 3.- The third case considers the split-film probe as, essentially, an x-configuration probe operated with linearized anemometry circuits. Starting with the power circuit equation, Eq. 12, we use a second exponential amplifier circuit to linearize the voltage directly in terms of U_{eff}. For n = 0.5:

$$E_{\ell_i} = K_{\ell_i} E_{P_i}^{1/n} = K_{\ell_i} K_{P_i}^2 U_{eff}\left(1 + \alpha_i \frac{U_2}{U_{eff}}\right)^2 \qquad (24)$$

Making the standard low intensity assumption (ignoring 2nd and higher order expansion terms), this becomes:

$$E_{\ell_i} = K_{\ell_i} K_{P_i}^2 \overline{U}_1\left[1 + \frac{u_1}{\overline{U}_1} + 2\alpha_i \frac{U_2}{\overline{U}_1}\right] \qquad (25)$$

which we recognize as the familiar x-probe equation. Indeed, for $\alpha_i = 0.5$ the sensitivity to transverse direction fluctuations is the same as for 45° inclined sensors. Figure 7 shows yaw calibration data obtained under similar

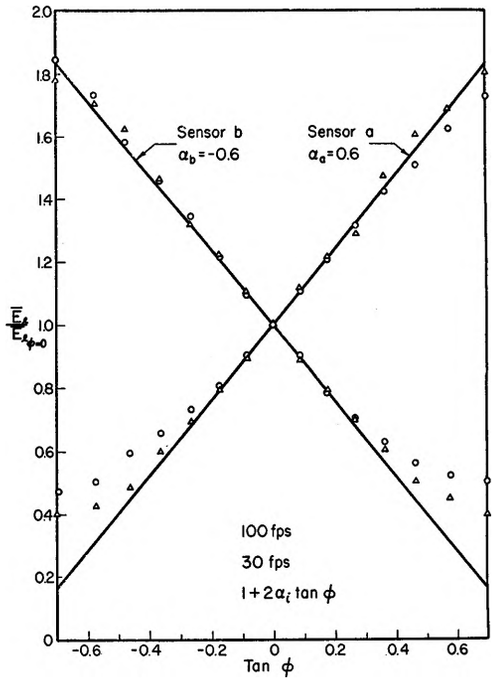

Figure 7 - Azimuthal Yaw Calibration for SF-6 in Air Flow with O.H.R. = 1.5 using Eq. 26

conditions as described under Case 2. For calibration purposes in steady flow, Eq. 25 is written:

$$E_\ell/E_{\ell_{\phi=0}} = 1 + 2\alpha_i \tan\phi \qquad (26)$$

The data can be seen to agree with this representation reasonably well in the yaw range $|\phi| \lesssim 20^o$ with $\alpha_i = \pm 0.6$. This α_i differs slightly from the value predicted by above analysis, $\alpha_i = \pm 0.47$, which is attributable to the uncertain form of the azimuthal heat flux distribution, Eq. 7. At angles larger than about 20°, second order effects become significant. The usefulness of this technique is thereby limited to applications where the transverse intensity, $u_2'/\overline{U}_1$, is less than about 0.2. Since in many instances of shear flow turbulence this criterion is met, the direct linearization technique is very appealing in view of its simplicity.

Assuming matched anemometry circuits and $\alpha_a = -\alpha_b$, the linearized voltages, Eq. 25, can be summed and differenced in the standard manner giving:

$$E_s = G_s(E_{\ell_a} + E_{\ell_b}) = 2\,G_s K_\ell K_P^2(\overline{U}_1 + u_1) = S_1(\overline{U}_1 + u_1) \qquad (27a)$$

and

$$E_d = G_d(E_{\ell_a} - E_{\ell_b}) = 4G_d K_\ell K_P^2 \alpha U_2 = S_2(\overline{U}_2 + u_2) \qquad (27b)$$

where the sensitivities S_1 and S_2 are determined by direct calibration in the velocity and yaw ranges of interest. Since $S_2 = 2\,\alpha\,(G_d/G_s)\,S_1$, it is not necessary to perform a yaw experiment to determine S_2 if a value for α is assumed. The mean and fluctuation components of the flow field are given by:

$$\overline{U}_1 = (1/S_1)\overline{E}_s;\quad u_1 = (1/S_1)e_s \qquad (28a)$$

and

$$\overline{U}_2 = (1/S_2)\overline{E}_d;\quad u_2 = (1/S_2)e_d \qquad (28b)$$

These response equations were used for turbulence measurements in a plane, separated shear layer using a 6-mil sensor (SF-6) as described below. A component block diagram is shown in Fig. 8.

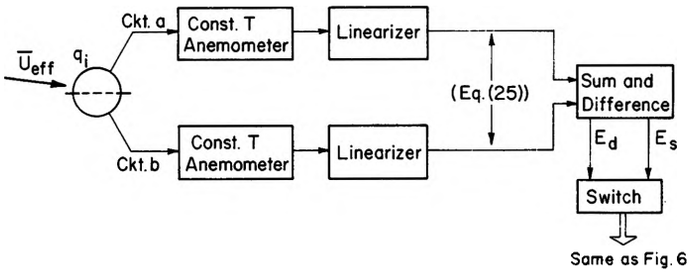

Figure 8 - Component Block Diagram for Case III

The techniques described show the versatility of the split-film (SF) probe to the experimenter based on his measurement and accuracy requirements. The operation of an SF probe will now be described.

EXPERIMENTAL RESULTS

Two split-film probes were obtained from Thermo-Systems, Inc. (TSI) to be used for shear layer turbulence measurements. The first was a cantilevered, upstream oriented probe having a 6-mil split-film sensor (designated SF-6) which was used for mixing layer turbulence measurements (Fig. 9). The second

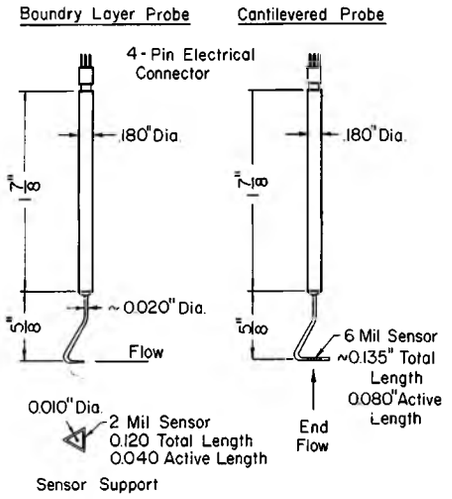

Figure 9 - Split-Film Probes Used for Shear Layer Turbulence Measurements

probe was obtained with a 2-mil sensor (SF-2) and was adapted for boundary layer measurements (Fig. 9). Two channels of TSI Model 1054B constant temperature anemometers were used. Additionally, squaring circuits, variable exponent amplifiers, and standard dc amplifiers having voltage offset capability were part of the basic electronic circuitry.

The cold resistances of each sensor of the SF-2 and SF-6 probes were about 20 Ω and 50 Ω, respectively. An overheat ratio of 1.5 was used. In the case of the SF-6 probe this necessitated an external modification to the decade resistors to extend their range, and this was provided by the manufacturer. The temperatures of the two film elements could be matched by operating one channel at a nominal overheat with the sensor shielded and measuring the "cold" resistance of the second channel. This resistance would then be used for operation of the second channel. Standard square-wave tests were used to optimize the bridge balance at the maximum flow rate of interest. The indicated response times were 20 μsec and 8 μsec for the SF-2 and SF-6 probes, respectively. There was no noticeable electronic coupling between channels for the SF-6 probe although slight coupling was observed for the SF-2 probe during the square wave tests.

Mixing Layer Measurements

The circuitry of Fig. 8 was employed for turbulence measurements in the two-stream mixing layer[4] using the SF-6 probe. Comparison was made with the results from carefully performed x-probe measurements; spatial resolution was excellent for each probe in this large mixing layer. Yaw calibration tests were run for the TSI 1241-T1.5 upstream oriented x-probe; the yaw sensitivities for the two wires were matched, and the apparent sensor angles of $\pm 40^\circ$ were used in the response equations. The x-probe response time was 4 μsec.

The turbulence measurements were made 22 inches downstream from initial mixing in the fully-developed region of a two-stream mixing layer. The medium was air; the primary stream velocity (U_a) was 100 fps and the secondary stream velocity (U_b) was 30 fps (velocity ratio $r = U_b/U_a = 0.3$). The mean velocity profiles measured with the two probes were in close agreement. However, the axial and transverse direction turbulence intensities measured with the SF-6 probe were significantly smaller than those obtained with the x-probe, as shown in Fig. 10. The differences were about 20% based on the accepted (and cross-

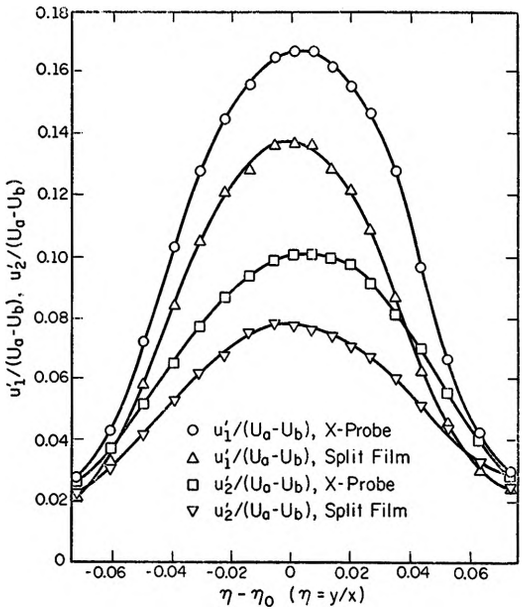

Figure 10 - Comparison of Turbulence Measurements in Two-Stream Mixing Layer Using Split-Film (SF-6) and X-Probes

checked) x-probe results. This discrepancy was attributed to the poor frequency response of the SF-6 probe in the turbulent flow field, moreso than could be rationalized by the difference in response times indicated by the square wave test. To examine this, detailed frequency response tests were performed on the SF probes under actual flow conditions.

Frequency Response

The SF sensors were subjected to sinusoidally oscillating air flow generated by both transitional wake flow and vortex shedding from circular cylinders. A range of mean velocities and cylinder diameters was used to produce the desired shedding frequencies. A TSI 1270-T1.5 hot-wire sensor (with response time = 7 μsec) was used as a standard for comparison of sensor responses. The hot-wire probe and the probe being tested were mounted in a tandem holding device and traversed together in the flow field, thereby assuring maximum relocation

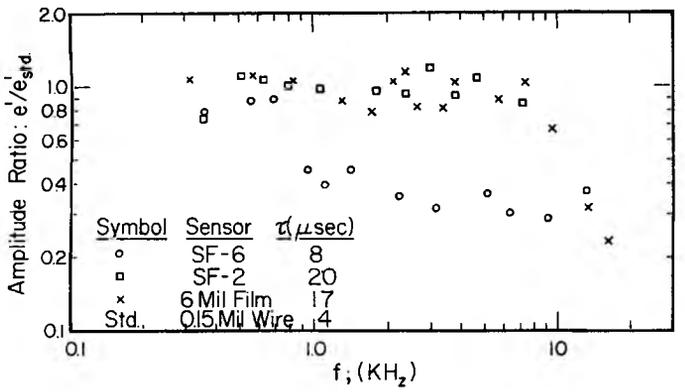

Figure 11 - Frequency Response of Film Sensors in Fluctuating Flow Field

accuracy. Even with this precaution, the scatter in results (Fig. 11) reflects principally the positioning difficulties in the very small vortex fields generated. These difficulties are particularly pronounced for the relatively large SF-6 sensor with its possible influence on the vortices. The estimated uncertainty in individual data points is ± 20%. In general, however, the magnitudes and trends are felt to be reliable despite this scatter.

The results indeed verify an abnormal response behavior for the SF-6 probe. The amplitude ratio drops from unity (within experimental uncertainty) at frequencies above 700 Hz to an approximately constant level between 0.3 and 0.4 at higher frequencies. A cumulative energy distribution of hot-wire signals in the mixing layer turbulence indicated about 20% of the energy was contained in the spectral range above 700 Hz. The measurements with the SF-6 probe were small by this same amount, and it appears plausible that this frequency response behavior may be the cause.

An explanation for the observed response behavior is not apparent, however. A comparison was made with an ordinary 6 mil sensor operated under identical experimental conditions. Its response, shown in Fig. 11, is the same as that of the hot-wire, being limited at high frequencies only by the electronic response time and the flow transit time over the sensor. This result, incidentally, does not invalidate (but rather tends to substantiate) the basic assumption stated earlier, i.e., that the heat flux distribution, Eq. 7, follows rapidly the local velocity vector in rotation about the cylinder. In the normally used orientation, film sensors should respond to U_{eff} as the hot wire does, and obtaining an amplitude ratio of unity as shown in Fig. 11 may be considered as evidence that this occurs within the appropriate frequency range of the sensors.

The SF-2 probe was tested in the same manner as the SF-6 probe and the results in Fig. 11 show unity amplitude ratio to at least 7 kHz. This indicates that the response difficulty experienced with the SF-6 probe is not inherent in the split-film concept nor in its electronic circuitry. However, no satisfactory explanation for the behavior of the SF-6 sensor is available.* The excellent response obtained with the SF-2 probe was gratifying after the earlier difficulties with the SF-6 probe and motivated us to proceed directly with the boundary layer measurements using this (SF-2) probe.

Boundary Layer Measurements

Turbulence measurements were made in a boundary layer developing along a test section wall in our low turbulence wind tunnel.[4] A 1/16-inch diameter trip wire and a 2-inch wide strip of coarse emery cloth were used for artificial thickening at the inlet, and the measurements were made at a location 60 inches downstream. The wind tunnel flow was undisturbed for an additional 4 feet past this station. The free stream velocity was 100 fps, and the boundary layer thickness, δ, was 1.0 inches. The probe location was zeroed with respect to the plexiglas surface using an image viewing technique. The closest approach to the wall was limited to 0.003 inches measured from the sensor axis. A TSI 1274-T1.5 hot-wire boundary layer probe was used for comparison with the SF-2 probe for axial velocity measurements.

Mean velocity profiles measured with the two probes were in excellent agreement. The axial turbulence intensities $u_1'/\overline{U}_\infty$ (Fig. 12) were in good

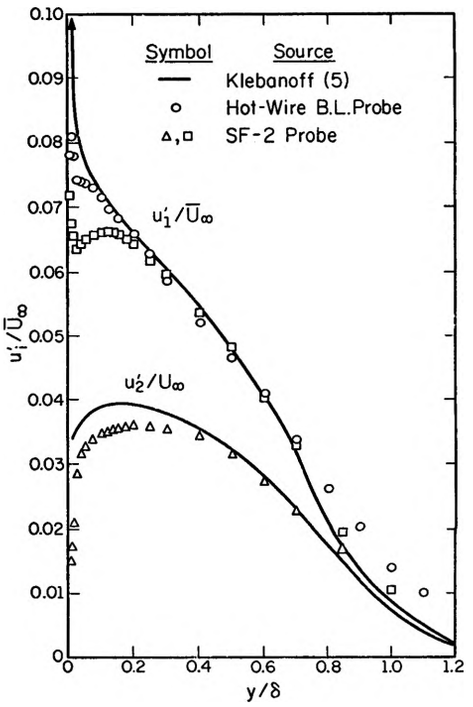

Figure 12 - Comparison of Flat Plate Boundary Layer Turbulence Data Using Split-Film and Hot-Wire Sensors

agreement with each other and with Klebanoff's data at $y/\delta \geq 0.2$. Closer to the wall the SF-2 data peaked while the hot-wire data showed continued rise agreeing more closely with Klebanoff's measurements. Those data also began deviating from Klebanoff's data, however, at about $y/\delta = 0.05$. The reason for the disagreement with his data may be the finite axial pressure gradient known to exist in the wind tunnel, but without further more detailed study of this effect in the flow facility this is not certain. The local turbulence intensities were not in excess of 0.2 and the band width of the SF-2 probe was more than adequate to cover the spectral range. Although the u_1' results do not show the agreement expected, it is noteworthy that the transverse intensity u'_2/U_∞ is in reasonable agreement with Klebanoff's data throughout the boundary layer. The trends shown are identical, although the magnitudes, again, are too small. Both sets of data peaked between y/δ values of 0.15 and 0.20, and the peak amplitudes were 0.036 and 0.039 for the SF-2 probe and Klebanoff's results, respectively.

The shear stress measurements showed a smooth trend and little scatter, but the peak value of $-\frac{\overline{u_1 u_2}}{U_\infty^2} = 0.72 \times 10^{-3}$ is a factor of two smaller than Klebanoff's results due to both u_1 and u_2 being measured too small. The shear correlation coefficient took on an approximately constant value of $\overline{u_1 u_2}/(u_1' u_2') \approx 0.315$ inside $y/\delta = 0.7$; this compares with the theoretical value of 0.5 inside $y/\delta = 0.8$ indicated by Klebanoff.

In comparing the measured data with that of Klebanoff, the intent has been to show the similarity of trends rather than perfect numerical agreement.

* In an attempt to examine further the apparent discrepancy of the frequency response of SF-6, a set of frequency response tests were performed on a second SF-6 sensor after presentation of this paper. These are reported as an addendum.

This is a direct consequence of the choice of an existing experimental facility which unfortunately did not provide the ideal zero pressure gradient flow and had artifical initial thickening of the boundary layer. The effects of these with respect to the more ideal flow in which Klebanoff made measurements was not studied. This, in part, may explain some of the differences in experimental results.

In summary, we have succeeded in making two-dimensional turbulence measurements close to the wall in the turbulent boundary layer. The measurements showed no adverse effects of the proximity of the wall at distances greater than 10 sensor diameters (0.02 inches). The turbulence results obtained with the SF-2 probe were in only fair agreement with results obtained using a standard boundary layer probe and with Klebanoff's published data. In particular, the u_1-intensities showed an unexpected trend and low magnitudes as the wall was approached. The u_2' data agreed satisfactorily with Klebanoff's. The shear stress results, as would be expected from the low u_2' measurements, were also low. The correlation coefficient, while smaller than anticipated, showed the expected behavior.

SUMMARY AND CONCLUSIONS

The split-film anemometer sensor has been shown to have promise as a research tool for two-dimensional turbulence measurements. Its unique geometry makes it potentially superior to the conventional x-probe for boundary layer or other measurements where spatial resolution across mean shear regions is important. The quasi-static response equations which have been derived suggest techniques for operating the probe as well as interpreting its response in terms of flow field characteristics. The experimenter should, however, be cautioned that in its present state of development, the split-film sensor has a somewhat poorer frequency response than a standard 0.15-mil tungsten wire. Further, the frequency response is a sensitive function of mean velocity. Hence prior to use, adequate frequency response throughout the velocity range of interest should be verified.

ACKNOWLEDGEMENTS

The authors gratefully acknowledge the loan from Thermo-Systems Inc. of St. Paul, Minnesota of the (SF-6) split-film sensors. Thanks are also extended to H. P. Planchon, Jr. for performing the additional frequency response tests following presentation of this paper.

SYMBOLS

A	defined by Eq. 6
A_i	surface area of sensor i
B	defined by Eq. 6
e	fluctuating component of anemometer voltage output
E	instantaneous total anemometer voltage output
$f(\phi)$	defined by Eq. 6
$f_i(\phi)$	defined by Eq. 9
G	system gain; defined by Eqs. 13, 14 and 15
$H(\phi)$	azimuthal distribution of the local convective heat transfer coefficient
h_i	average convective heat transfer coefficient of sensor i
$H'(\beta)$	defined by Eq. 7
I_i	current in sensor i
K_{ℓ_i}	calibration constant; defined by Eq. 24
K_{P_i}	calibration constant; defined by Eq. 12
n	exponent in Eq. 6
O.H.R.	sensor operating over-heat-ratio
Q_i	power dissipated by sensor i
r	velocity ratio, U_a/U_b
R_i	resistance of sensor i at T_{S_i}
Re	Reynolds number
S_i	anemometer voltage-to-velocity sensitivity
T_a	ambient fluid temperature
T_{S_i}	Temperature of sensor i
u_i	instantaneous fluctuating velocity component in x_i-direction
U_a	primary stream velocity for two-stream mixing layer
U_b	secondary stream velocity for two-stream mixing layer
U_{eff}	effective instantaneous cooling velocity
U_i	instantaneous total velocity component in x_i-direction
U_∞	free stream velocity above boundary layer
x_i	orthogonal co-ordinate directions; i = 1,2,3; (See Fig. 3)
$\hat{x}_i$	unit vector in the x_i-direction
α_i	defined by Eq. 9
δ	boundary layer thickness
ϕ, ϕ'	defined in Fig. 2
τ	sensor response time

Subscripts

a,b	sensor a and b designation
d	differencing related
ℓ	linearized operation related
p	product related
s	summing related

Other

$( )'$	root mean square of ( )
$\overline{( )}$	time average of ( )
$\vec{( )}$	total vector quantity of ( )
$\lvert ( ) \rvert$	absolute value of ( )

REFERENCES

1. Olin, J. G., and Kiland, R. B., "Split-Film Anemometer Sensors for Three-dimensional Velocity-vector Measurement," paper presented at Symp. on Aircraft Wake Turbulence, Sept. 1-3, 1970, Seattle, Washington.
2. Weber, D. P., and Jones, B. G., "Axial Heat Losses in Circular Cylinders and its Application to the Determination of the Azimuthal Convective Heat Transfer Coefficient with a Split-Film Anemometer Probe," Presented at the Winter Annual Meeting of A.S.M.E., Washington, D.C., Nov. 28-Dec. 2, 1971 and included in the Symposium Series Volume on "Fluid Flow and Heat Transfer at Low Reynolds Numbers".
3. Kreith, F., Principles of Heat Transfer. International Textbook Company, Scranton, Pa., 1963.
4. Spencer, B. W., and Jones, B. G., "Statistical Investigation of Pressure and Velocity Fields in the Turbulent Two-Stream Mixing Layer," AIAA Paper No. 71-613 (1971)
5. Klebanoff, P. S., "Characteristics of Turbulence in a Boundary Layer with Zero Pressure Gradient," NACA Rept. 1247 (1955).
6. Hinze, J. O., Turbulence, McGraw-Hill Book Co., New York, N.Y., 1959.

ADDENDUM

The unusual frequency response of SF-6 and the generally low values of turbulent intensities and shear stress measured with both the SF-6 and SF-2 sensors prompted further investigation of the split-film sensor. In these experiments the amplitude ratio of a second SF-6 sensor with a boundary layer configuration was measured in wake generated turbulence and the variation of the square wave response of SF-6 was studied as a function of mean velocity.

The experimental setup previously described was used and the anemometry was optimized at 100 fps steady mean flow for both these tests. The varia-

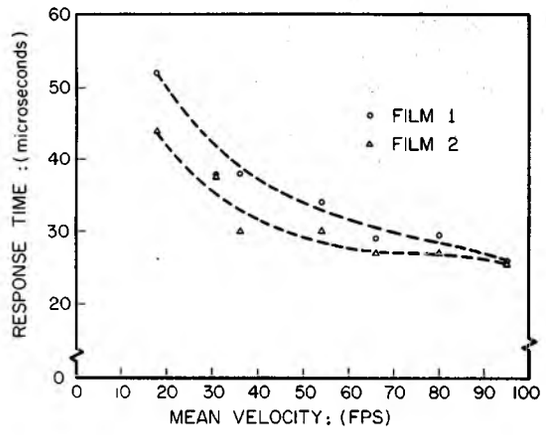

Figure A-1 - Response Time of SF-6 to Square Wave Test vs Mean Fluid Velocity

tion of response time with mean velocity, shown in Fig. A-1, was obtained by direct measurement using a square wave perturbation. Here we are defining the response time as the time interval from the square wave input until the system response has decayed to 1/3 of its maximum value. That response time decreases with mean velocity is well known (see Hinze[6]), but the amount of decrease demonstrated in Fig. A-1 was surprising.

The spectral density of SF-6 was generated by a 1/10 octave band pass analyzer and compared with that of a TSI-T1.5 sensor. The two sensors were alternately positioned in the same location in the center of the turbulent wake of a 1/4 inch rod. This turbulent field produced a spectrum with frequencies of interest and was of sufficient size and magnitude so that sensor location and electronic noise errors were negligible. The amplitude ratio was computed from

$$A(f) = \frac{e'_{SF-6}(f)}{e'_{T1.5}(f)} \frac{S_{T1.5}}{S_{SF-6}}$$

where the $S_{T1.5}$ and S_{SF-6} are the sensitivities of the T1.5 and SF-6 sensor circuits, respectively. A(f) is presented in Fig. A-2 which shows the decrease in frequency response of SF-6 with decreasing velocity. This figure also demonstrates that at the high frequencies found in air, this instrument will introduce significant errors in measured turbulence intensities. However, no sharp change in the sensor's response at about 700 Hz was noted, which tends to confirm the suspicion that the use of discrete shedding frequencies from small rods for the relatively large SF-6 sensor is not satisfactory. Since varying mean flow speed also is necessary in such tests, this can adversely affect the calibration.

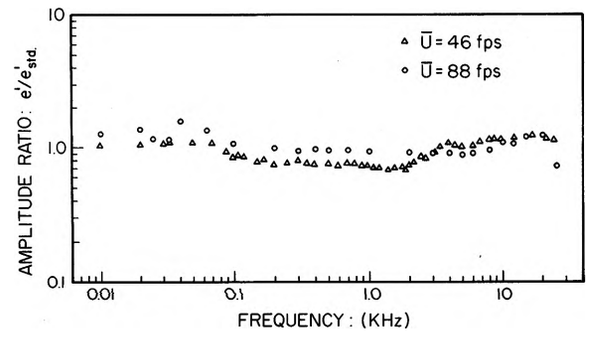

Figure A-2 - Frequency Response of SF-6 in the Wake of 1/4-inch Diameter Rod

DICUSSION

S. KLINE (Stanford University): Regarding the failure of the 6-mil probe response, did you try to estimate whether that was due to film lag or substrate lag? Do you have any idea why that falls off?

JONES: No, we didn't examine this in detail. However, we suspect the individual film. I think perhaps the people from TSI might indicate whether or not they have heard of anyone else running into this problem with a 6-mil, but we used one probe and that was the response we had. (Subsequent to this presentation we examined another 6-mil sensor with similar results and now suspect that the use of shedding frequencies to test the frequency response is not acceptable for this size sensor.)

S. KLINE: I suspect that it either must be substrate or the fact that the probe is bigger and therefore it takes a longer time in boundary layer residence for the fluid to get around the thing, and hence there is an inherently lower fluid film response.

JONES: I think that if that was true we would have probably seen the response drop off even further. However, the response reduced sharply and then held that level as we went on out in frequency.

F. ERIAN (Clarkson College of Technology): Did you estimate the effect of axial cooling on this wire since it has such a large surface area? Suppose the effect of velocity is not really normal to the axis of the wire or along the axis of the wire? Or suppose you have a reasonable fluctuation along the axis of the probe? With a large surface area, would you still say that this would be negligible as in a hot-wire probe?

JONES: We oriented the probe so that the normal to the azimuthal direction was perpendicular to the flow; the end loss effects are then balanced.

However we obviously don't have the advantageous length to diameter ratio we do in a hot wire and this makes a difference. If we get cooling from fluctuations in the axial direction, errors will result. Of course we can effectively calibrate in a smooth flow and then estimate the order of the error. The order of the error is relatively small. Very small, particularly if the probe axis is normal to the mean flow. If it is at an angle to the mean flow, then one must go back and examine the k for the sensor's angle to the mean flow.

F. ERIAN: Could you say that the error in the quantitative results in the boundary layer would be due to axial cooling?

JONES: I don't think so because we effectively calibrated in the steady mean flow stream and so in effect we get our calibration constants under the flow conditions. Normally, as long as the axial loss is symmetric, this effect is taken into account in the calibration.

T. HOULIHAN (Naval Post Graduate School): You mentioned that a good portion of the error may arise from probe location. How did you locate the probes?

JONES: In the boundary layer we could locate the probe within 0.001 inch or so by using a reflective light technique and then traversing away from the surface in a well-controlled manner.

I referred to probe location errors when looking at the frequency response, not in either experimental study. There we were locating the probe behind a cylinder in a smooth flow and looking at the wake. In order to get the high frequencies that were required we had to use small cylinders. It was then very difficult to relocate the probe at exactly the same spot. Instead the sensors were mounted together and simultaneously traversed on through the wake. Now in order to set different frequency ranges we had to keep changing shedding sizes of cylinder and mean flow velocities. As a result we had to effectively relocate the probes.

T. HANRATTY (University of Illinois): How close did you get to a wall in these measurements and what limited the distance that you could get to the wall?

JONES: You obviously can't traverse right to the wall because this will result in an interference problem. The flow will accelerate between the sensor and the wall, and the acceleration will be preferentially on the wall side giving non-interpretable results. What we did was approach the wall monitoring the U-component until it effectively deviated from the smooth trend of the data. We could go much closer to the wall, ideally, with the 0.15-mil wire. We found that when we got within 3 or 4 diameters, deviations from smooth trends resulted indicating that we shouldn't interpret our results any closer. Certainly if we stay outside of 10 diameters we know we are not being influenced at all. However, we think we can go closer than that, say within 5 to 6 mil of the wall for the 2-mil sensor.